

PHOTOMETRY AND SPECTROSCOPY OF OLD, OUTER DISK STAR CLUSTERS:  
VDB-HAGEN 176, BERKELEY 29 AND SAURER 1PETER M. FRINCHABOY<sup>1,2,3</sup>, RICARDO R. MUÑOZ<sup>1</sup>, RANDY L. PHELPS<sup>3,4,5,6</sup>,  
STEVEN R. MAJEWSKI<sup>1,2</sup>, AND WILLIAM E. KUNKEL<sup>7</sup>*Draft version September 7, 2018*

## ABSTRACT

It has been previously proposed that some distant open clusters in the Milky Way may have been accreted during a dwarf galaxy merger, perhaps associated with the same event that led to the formation of the Galactic anticenter stellar structure (GASS), also known as the “Monoceros Ring”. We have obtained *VI* and Washington+*DDO51* photometric and medium resolution ( $R \sim 8000$ ) multi-fiber spectroscopic data for the three distant old open clusters Berkeley 29, Saurer 1, and vdB-Hagen 176 (BH 176). These clusters are spatially coincident with GASS, but radial velocities and spectroscopic metallicities had not been available during previous studies of the GASS candidate cluster system. Similar data for the clusters Berkeley 20 and Berkeley 39 have been obtained for calibration purposes. We provide the first *reliable* radial velocity for BH 176 ( $V_{\text{helio}} = 11.2 \pm 5.3 \text{ km s}^{-1}$ ). We also find that  $V_{\text{helio}} = +95.4 \pm 3.6$  and  $+28.4 \pm 3.6 \text{ km s}^{-1}$ , for Saurer 1(A) and Berkeley 29, respectively. We show that  $\alpha$ -enhanced isochrones, while spectroscopically motivated, provide a poor fit to Be29 in contrast to previous findings. We find that the clusters Berkeley 29 and Saurer 1 are consistent with the previously reported characteristics for GASS candidate clusters and the GASS stellar stream as derived from M-giant observations. However, the radial velocity and photometric metallicity ( $[\text{Fe}/\text{H}] \sim 0.0$  dex) for BH 176 suggests that a connection of this cluster with the putative GASS cluster system is unlikely. We reassess the age-metallicity relation for the most likely members of the GASS clusters system for which spectroscopic metallicities are now available.

*Subject headings:* Galaxy: structure – Galaxy: disk – galaxies: interactions – Galaxy: open clusters and associations: individual (Berkeley 20, Berkeley 29, Berkeley 39, Saurer 1, BH 176) – Galaxy: globular clusters: individual (BH 176)

## 1. INTRODUCTION

Frinchaboy et al. (2004, hereafter F04) noted that the outermost open clusters in the Milky Way seem to lie in a string-like configuration that can be fit to an orbital plane coincident with the Galactic anticenter stellar structure (GASS). The presence of this arc-like structure was inferred from excesses of various types of stars (Newberg et al. 2002; Yanny et al. 2003; Ibata et al. 2003; Majewski et al. 2003; Crane et al. 2003; Rocha-Pinto et al. 2003, 2005) beyond the apparent limit of the Galactic disk, and has also been used to argue for the presence of a distinct, extended stellar structure wrapping around the disk at low latitudes. The feature has been referred to as the “Monoceros Ring” (Newberg et al. 2002; Yanny et al. 2003) or GASS (Majewski et al. 2003; Rocha-Pinto et al. 2003; Crane et al. 2003). However, because of its unfortunate location behind considerable extinction, the system’s true shape, orientation, extent, etc. have been difficult to ascertain.

Even the location of the structure’s center (presumably corresponding to a “nucleus”) remains uncertain and controversial. For example, this stellar stream has been argued to be associated with the postulated Canis Major (Ibata et al. 2003; Martin et al. 2004) or Argo dwarf galaxies (Rocha-Pinto et al. 2005).

Previous work (Crane et al. 2003) on this stellar arc has determined some characteristics including: (1) a velocity-longitude trend that indicates a slightly non-circular orbit, (2) a velocity dispersion that is smaller than even that of disk stars, and (3) a wide metallicity spread from  $[\text{Fe}/\text{H}] = -1.6 \pm 0.3$  dex (Y03) to at least  $[\text{Fe}/\text{H}] = -0.4 \pm 0.3$  dex. F04 found that at least five globular clusters and one open cluster (Tombaugh 2) have positions and radial velocities (RVs) suggesting an association with GASS (see also Martin et al. 2004; Frinchaboy et al. 2005), but pointed to other clusters with spatial coincidence with GASS that still have unknown RVs. As a result, we sought to derive the kinematics and chemistry for these other clusters. In this work, the clusters Berkeley 29 (Be29), Saurer 1 (Sa1)<sup>8</sup>, and vdB-Hagen 176 (BH176) from the F04 list of postulated GASS clusters are investigated. Table 1 gives the positional data for these clusters, as well as for old, outer open clusters Berkeley 20 (Be20) and Berkeley 39 (Be39), which we also observed as metallicity calibrators. Medium resolution spectra for all five clusters are used to determine their bulk RVs and metallicities via measurement of the Ca II infrared triplet lines. These data are used to test whether these clusters are consistent with the observed dynamical and chemical trends of the GASS system. While Yong et al. (2005) and Penarrubia et al. (2005) suggest the

Electronic address: pmf8b, rrm8f@virginia.edu, phelps@csus.edu, srm4n@virginia.edu, kunkel@jeito.lco.si

<sup>1</sup> Department of Astronomy, University of Virginia, P.O. Box 3818, Charlottesville, VA 22903-0818.

<sup>2</sup> Visiting Astronomer, Cerro Tololo Inter-American Observatory, National Optical Astronomy Observatory, which is operated by the Association of Universities for Research in Astronomy, Inc. (AURA) under cooperative agreement with the National Science Foundation.

<sup>3</sup> Visiting Astronomer, The Observatories of the Carnegie Institution of Washington, 813 Santa Barbara Street, Pasadena, CA 91101.

<sup>4</sup> Department of Physics & Astronomy, California State University, Sacramento, 6000 J Street, Sacramento, CA 95819-6041.

<sup>5</sup> Department of Physics, University of California, Davis, 1 Shields Avenue, Davis, CA 95616 (on leave).

<sup>6</sup> On assignment to National Science Foundation, 4201 Wilson Boulevard, Arlington, Virginia 22230.

<sup>7</sup> Las Campanas Observatory, Casilla 601, La Serena, Chile.

<sup>8</sup> Originally described as Saurer A in Frinchaboy & Phelps (2002) and Carraro & Baume (2003).

TABLE 1  
CLUSTER BASIC PARAMETERS

Cluster	$\alpha_{2000.0}^a$	$\delta_{2000.0}^a$	$l(^{\circ})^a$	$b(^{\circ})^a$	Diam. <sup>a</sup>	$E(V-I)_{pub}$	Ref
vdB-Hagen 176 (BH176)	15:39:05.4	-50:03:01.7	328.4100	+ 4.3418	2.3'	0.70	1
Berkeley 20 (Be20)	05:32:37.0	+00:11:30.0	203.4803	-17.3711	2.0'	0.16	2
Berkeley 29 (Be29)	06:53:04.2	+16:55:39.0	197.9493	+ 7.9802	2.0'	0.10	3
Berkeley 39 (Be39)	07:46:51.0	-04:40:30.0	223.5465	+10.0915	7.0'	0.11	4
Saurer 1 (Sa1)	07:20:56.0	+01:48:29.0	214.6894	+ 7.3862	1.3'	0.18	5

REFERENCES. — (1) Phelps & Schick (2003); (2) MacMinn et al. (1994); (3) Tosi et al. (2004); (4) Carraro et al. (1994); (5) CBVMPR

<sup>a</sup>Fundamental data from Dias et al. (2002)

metallicity and RV data are insufficient to prove membership in GASS, they are sufficient to identify clusters with properties inconsistent with those observed for GASS.

In §2 we analyze photometry for the clusters Be20, Be29, Be39, Sa1, and BH176. This photometry is used to select targets for spectroscopy. In §3, we discuss the spectroscopic observations and use RVs derived from the spectra to determine the clusters' bulk RVs. The derived mean cluster RVs are used to clarify the positions of the giant branches of the clusters in the color-magnitude diagram and compare our work to previous studies in §4. Finally in §5, we explore each cluster's likelihood of belonging to GASS and discuss the implications these clusters have for GASS and open cluster studies in the Galaxy in general.

## 2. PHOTOMETRY OF DISTANT OPEN CLUSTERS

The clusters Be29 and Sa1 were imaged in the Cousins  $V$  and  $I$  filters with the University of Virginia's 40 inch telescope at Fan Mountain Observatory (FMO). We also make use of  $VI$  photometry of BH176, taken with the LCO DuPont 2.5m; these data are described more fully in Phelps & Schick (2003). The details of the  $VI$  observations are listed in Table 2. The Fan Mountain SITe CCD has  $2048 \times 2048$  pixels that are  $24 \mu\text{m}$  square, resulting in a pixel scale of  $0.367 \text{ arcsec pixel}^{-1}$  and a field of view of  $12.67 \text{ arcmin}$  on a side. Be20, Be 39 and Sa1 were also observed using Washington ( $M$ ,  $T_2$ )+ $DDO51$  filters<sup>9</sup> with the FMO 40 inch and with the 40 inch Swope telescope at the Las Campanas Observatory (LCO; see Table 3). The Swope CCD has  $2048 \times 2048$  pixels that are  $24 \mu\text{m}$  square, yielding a pixel scale of  $0.697 \text{ arcsec pixel}^{-1}$ , for a field of view of  $23.7 \text{ arcmin}$  on a side. All exposures were obtained under photometric conditions. During each run, standard stars ( $VI$  from Landolt 1992, Washington+ $DDO51$  from Geisler 1996) were observed at various airmasses between airmasses 1 and 2 for photometric calibration of the data (see §2.2 below).

The imaging data have been reduced with the *IRAF*<sup>10</sup> CCDRED package, following standard techniques as described in the *IRAF* CCDPROC documentation. Instrumental magnitudes were measured with the DAOPHOT and ALLSTAR packages, using the point-spread function method (Stetson 1987). These magnitudes were transformed to the Landolt (1992) standard-star system (for  $V$  and  $I$  observations) and to the Geisler (1996) standard system (for data in the

<sup>9</sup> The  $T_2$  and  $I$  filters used for this study were identical; hereafter we will refer to these filters as  $I$ .

<sup>10</sup> IRAF is distributed by the National Optical Astronomy Observatories, which are operated by the Association of Universities for Research in Astronomy, Inc., under cooperative agreement with the National Science Foundation.

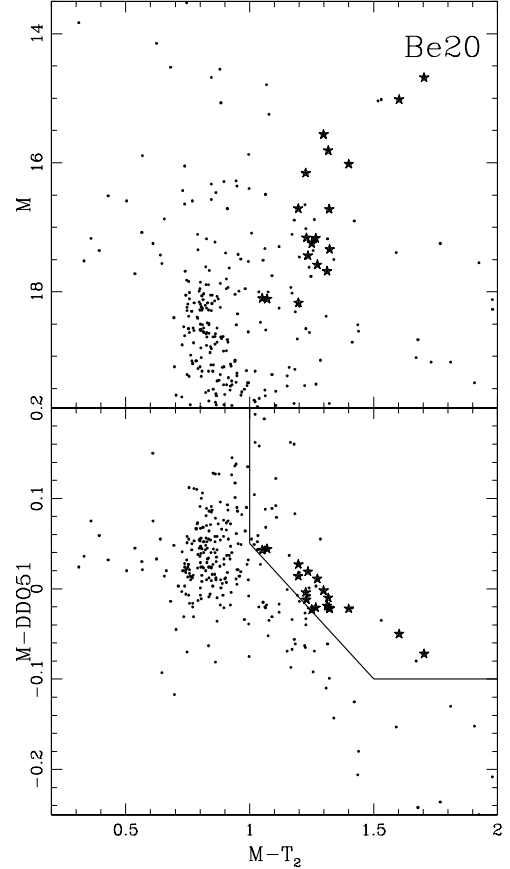


FIG. 1.— Dereddened Be20 Washington+ $DDO51$  photometry color-magnitude and color-color diagrams used for spectroscopic target selection. Stars selected as open cluster giant candidates from the Washington+ $DDO51$  color-color diagram are denoted with stars (★).

Washington+ $DDO51$  system). The data for BH176 are taken from Phelps & Schick (2003) and the errors are presented there. For the clusters Be20 and Be39, observed only with Washington+ $DDO51$  photometry, transformation equations from Majewski et al. (2000) were used to estimate  $V$  and  $V-I$ . Figures 1–3 show the  $M$ ,  $M-I$  color-magnitude diagram (CMD) and  $M-DDO51$ ,  $M-I$  color-magnitude diagram (CMD) for the clusters Be20, Be39 and Sa1.

### 2.1. Selection of Candidates for Spectroscopic Follow-up

Washington  $M$ ,  $I$ , and  $DDO51$  photometry can be used to discriminate between late-type dwarf and giant stars (Majewski et al. 2000) by calibrated  $(M-I, M-DDO51)_o$  color-color

TABLE 2  
VI PHOTOMETRY OBSERVING RUNS

Cluster	Telescope	Pixel Scale (arcsec pixel <sup>-1</sup> )	UT date	Exposures	
				V	I
BH176	LCO 2.5-m	0.259	1998 Jun 30	<sup>a</sup>	<sup>a</sup>
Be29	FMO 1.0-m	0.367	2003 Nov 21	1 × 900s	1 × 900s
Sa1	FMO 1.0-m	0.367	2004 Nov 21	1 × 900s	1 × 600s

<sup>a</sup>Photometry from Phelps & Schick (2003).

TABLE 3  
WASHINGTON+DDO51 PHOTOMETRY OBSERVING RUNS

Cluster	Telescope	Pixel Scale (arcsec pixel <sup>-1</sup> )	UT date	Exposures		
				M	I	DDO51
Be20	LCO 1.0-m	0.697	2000 Dec 05	1 × 120s	1 × 120s	2 × 420s
Be39	LCO 1.0-m	0.697	2000 Dec 05	1 × 120s	1 × 120s	2 × 420s
Sa1	FMO 1.0-m	0.367	2004 Feb 28	1 × 900s	1 × 600s	2 × 1800s

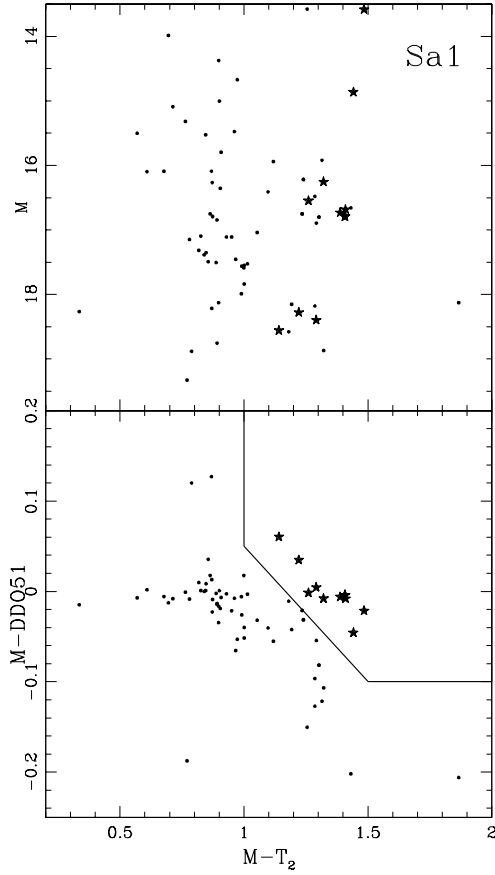


FIG. 2.— Same as Figure 5 for Sa1.

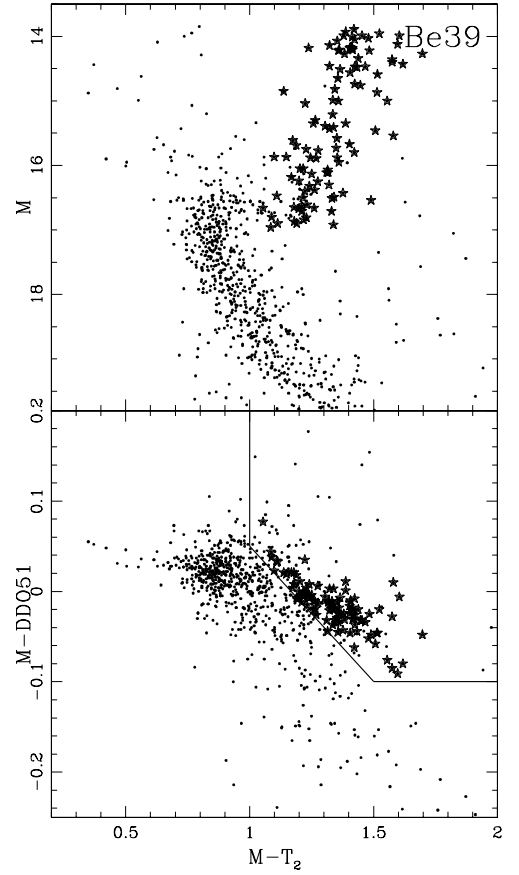


FIG. 3.— Same as Figure 5 for Be39.

diagrams. However to apply this technique, an estimate of the foreground extinction is necessary to correct the photometry to standard magnitudes. Literature values (presented in Table 1) have been adopted to implement this color-color based separation technique. We transform  $E(V-I)$  into  $E(B-V)$  using the relation derived by Dean et al. (1978). Finally, Majewski et al. (2000) provides relations to obtain  $E(M-DDO51)$ ,

$E(M-I)$  and  $A(M)$  based on  $E(B-V)$  and the ratio  $R_V = 3.1$  for the selective to total absorption.

Again, Figures 1–3 show the derived  $(M, M-I)$  CMDs with their respective  $(M-I, M-DDO51)_0$  color-color diagrams for the clusters Be20, Be39, and Sa1. The Washington color-color “giant region” is selected to separate giant stars from dwarf stars based on their surface gravity, as described in Ma-

TABLE 4  
SUMMARY OF RV STANDARD OBSERVATIONS

Star/Sp type	Fiber	TDR	$V_r$ (km s <sup>-1</sup> )	$\sigma_v$
HD 18884 (M1.5IIIa)	014	39.82	-26.50	1.28
	025	39.04	-26.27	1.47
	028	30.71	-27.14	1.19
	045	35.45	-26.38	1.38
	074	37.98	-26.96	1.44
	086	26.87	-26.29	1.51
	099	41.07	-26.33	1.44
	103	34.91	-26.23	1.42
	118	33.42	-26.15	1.20
	Average		-26.47	0.34
	IAU Value		-25.8	0.1
	Difference		-0.7	
HD150798 (K2II-III)	008	46.36	-3.41	1.05
	019	47.99	-3.04	0.96
	033	35.22	-2.77	1.25
	074	40.52	-5.10	1.63
	091	40.48	-3.21	0.91
	099	42.19	-3.10	1.13
	127	34.52	-3.08	1.23
	Average		-3.39	0.78
	IAU Value		-3.7	0.2
	Difference		+0.3	
HD157457 (G8III)	020	43.81	17.78	0.81
	034	34.79	17.05	0.66
	044	35.51	16.82	0.73
	045	34.56	17.50	1.37
	116	34.56	17.88	0.61
	125	30.61	18.43	1.17
	135 <sup>a</sup>	11.41	22.46	2.09
	Average		17.48	0.32
	IAU Value		17.4	0.2
	Difference		+0.1	
HD161096 (K2III)	030	42.29	-12.29	1.04
	038	35.49	-12.29	0.98
	039	37.83	-12.45	1.07
	040	38.85	-11.56	0.97
	048	31.59	-12.45	1.00
	057	28.02	-12.41	0.75
	077	41.44	-12.21	1.12
	098	43.22	-12.94	0.88
	104	42.25	-12.69	0.76
	110	39.67	-12.03	1.05
	Average		-12.33	0.37
	IAU value		-12.0	0.1
	Difference		-0.3	

<sup>a</sup>Due to poorer than average  $S/N$  this spectrum was not included in these calculations.

jewski et al. (2000). For this project, we define the following boundaries of the “giant region” for dereddened photometry:

$$(M-D) \geq -0.3(M-I) + 0.35 \text{ for } 1.0 \leq (M-I) < 1.5$$

$$(M-D) \geq -0.15 \text{ for } 1.5 \leq (M-I) \leq 2.0 \quad (1)$$

Stars that fall within the “giant box”, are within  $4'$  of the cluster center ( $7'$  for the larger Be39), and are brighter than the cluster main sequence turn off (MSTO) are denoted by stars (★).

### 3. RADIAL VELOCITIES OF DISTANT OPEN CLUSTERS

#### 3.1. Data Collection and Reduction

Spectroscopic data for cluster stars were collected on UT 2004 March 4–5 using the Hydra multi-fiber spectrograph on the 4-meter Blanco telescope at Cerro Tololo Intra-American Observatory. The spectra cover  $\lambda = 7800\text{--}8800\text{\AA}$  with an instrumental spectral resolution of  $R \sim 8000$ , or  $1.2\text{ \AA}$  per resolution element. To provide RV calibration, four RV standards were also observed, where each “observation” of an RV

standard entails sending the light down 7–10 different fibers, yielding many dozens of individual spectra of RV standards (see Table 4). For wavelength calibration, the “Penray” (HeNeArXe) comparison lamp was observed for every fiber setup.

To get spectra of as many members as possible in these compact star systems (diam.  $\sim 2'$ , see Table 1), we selected as primary targets cluster red giant branch (RGB) candidates from the cluster CMD. For clusters with Washington  $M$ ,  $I$ , and  $DDO51$  photometry, these RGB candidates were selected based on the CMD and their location in the  $(M-I, M-DDO51)_o$  color-color diagram, as described in §2.1 (i.e., the stars marked with star symbols [★] in Figures 1–3). These stars are the primary targets for spectroscopic observation, with stars within  $2'$  of the cluster center ( $R_{cluster}$ ) having the highest priority for observation. Since the Hydra spectrograph has “fiber packing” limitations (i.e., there is a minimum finer spacing of  $2.5''$ ), some fibers were placed on “extra” red giant branch candidates (ERGB) selected from  $2' < R_{cluster} < 4'$  (see Table 5), and to fill yet more fibers we also observed many non-RGB-selected stars in the surrounding field in a search for additional cluster members. Also, red clump (RC) and horizontal branch (HB) candidates were observed in Be20 and BH176. Spectroscopic targets for Be 29 and BH176 (clusters for which we were unable to obtain Washington photometry) were selected using the CMD of the inner  $4'$  of the cluster, with the RC stars for BH176 having the highest priority. We also “filled” fibers for these clusters in the manner described above. The small numbers of stars observed in some fields results from a combination of poor observing conditions, which yielded low  $S/N$  in the observations for some stars, as well as the limitation of the number of Hydra fibers that can be packed in a small area.

Preliminary processing of the two-dimensional images of the fiber spectra was undertaken using standard *IRAF* techniques as described in the *IRAF* CCDRED documentation. After completing the basic processing, the spectra were reduced using standard routines as listed in the DOHYDRA documentation.

#### 3.2. Radial Velocity Determination

All radial velocities ( $V_r$ ) were derived using *IRAF*’s FXCOR package, which was first used to determine RVs for the standard stars. The RVs of standard stars were measured by cross-correlating each Fourier-filtered standard star spectrum against every other. The resulting RVs for each individual spectra were averaged and the standard deviation measured; the results are presented in Table 4. As may be seen, the derived RVs for the standard stars are all within  $1\text{ km s}^{-1}$  of the IAU values.

We determine our RV errors from the prescription described in Vogt et al. (1995), which is based on analysis of repeated standard star spectra (Table 4). The Tonry–Davis Ratio (Tonry & Davis 1979, TDR) for each spectrum, measured from FXCOR, scales approximately with  $S/N$ , which allows us to determine the radial velocity error using the following equation:

$$\text{Error}(V_r) = \frac{\alpha}{(1 + \text{TDR})} \quad (2)$$

where  $\alpha$  is a constant calibrated by the standard star data. Average velocity uncertainties for the individual Hydra standard spectrum are  $\sigma_v \sim 1\text{ km s}^{-1}$  for standard star spectra with  $\text{TDR} > 25$ , which is  $S/N \geq 20$ . The cumulative  $\chi^2$  statistic for the repeat standard spectrum RV measures is  $\Sigma(1 + \text{TDR}_i)^2(V_{r,i} - \langle V_r \rangle)^2 / \alpha^2$ , where  $\langle V_r \rangle$  refers to the mean

TABLE 5  
SPECTROSCOPY OBSERVING STATISTICS

Cluster	Exposures	# Observed <sup>a</sup> (total/RGB)	# RV Stars <sup>b</sup> ( $S/N > 3$ )	UT date
BH176	$5 \times 1800s$	34/10 <sup>c</sup>	19/ 7 <sup>c</sup>	2004 Mar. 4
Be20	$4 \times 1800s$	38/12	20/ 4	2004 Mar. 5
Be29	$4 \times 1800s$	41/13	25/ 9	2004 Mar. 4
Be39	$5 \times 1800s$	68/39	54/36	2004 Mar. 5
Sa1	$4 \times 1800s$	24/12	11/ 4	2004 Mar. 4

<sup>a</sup>Total number of stars observed spectroscopically divided into two samples. 1) All stars. 2) Those stars selected as candidate RGB members from the cluster CMD (see §2.3).

<sup>b</sup>Number of stars with sufficient  $S/N$  to obtain an RV measurement.

<sup>c</sup>For BH176, “RGB” includes both RGB and RC stars.

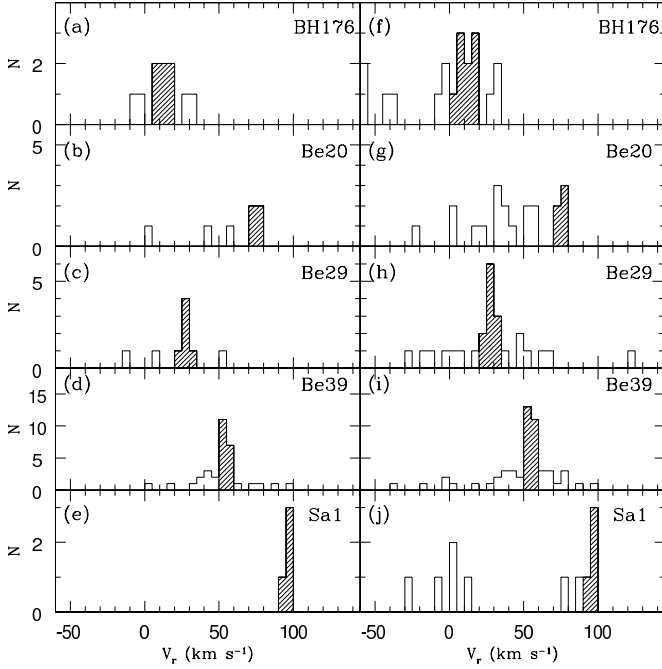


FIG. 4.— RV histograms for cluster stars observed, panels (a–e) show photometrically selected RGB and RC stars from Washington+DDO51 color-color selection (b,d,e) or from CMD selection in the cluster core (a,c), with shaded area denote selected members. Panels (f–j) show RVs for all stars observed used to find “new” member stars. NOTE: histogram bins are  $5 \text{ km s}^{-1}$  wide.

velocity and  $V_{r,i}$  the velocity of the standard star corresponding to the  $i$ th observation. We determine  $\alpha$  by finding the value of  $\chi^2$  where the probability of exceeding it by chance is 50% (defined as  $\chi_{50}^2$ ), which approximates  $1\sigma$  errors. The standard star spectra (Table 4) provide a data set with 29 degrees of freedom. From standard tables, we find that  $\chi_{50}^2 = 28.336$  for 29 degrees of freedom, which yields  $\alpha = 25.4$ .

Analysis of the cluster star spectra were also measured with FXCOR, and errors were determined from the measured TDR using the  $\alpha$  derived above. The photometric data and heliocentric RV ( $V_r$ ) and error (Error  $V_r$ ) measurements for cluster target stars with a TDR greater than 5 ( $S/N \geq 3$ ) are presented in Tables 6–10, along with information on the target selection described below in §3.3. The measured cluster star RVs are analyzed to determine membership in each cluster.

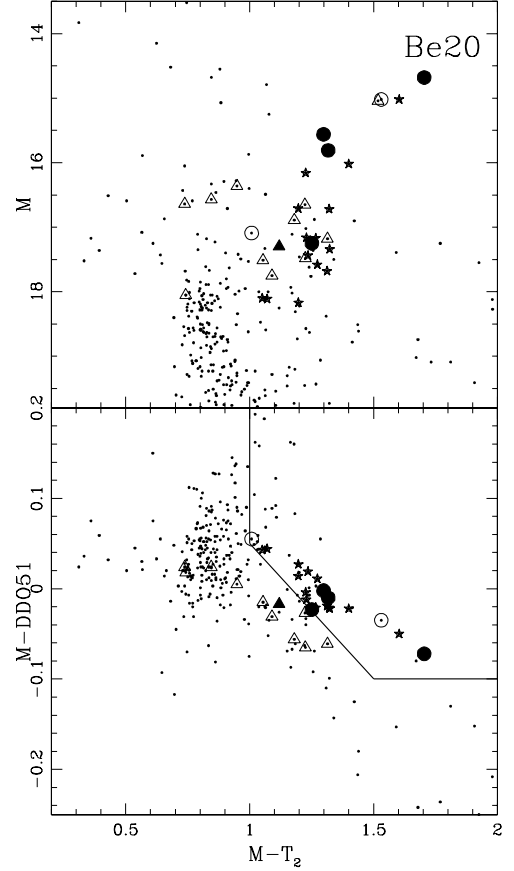


FIG. 5.— Dereddened Be20 Washington+DDO51 photometry color-magnitude and color-color diagrams. Stars selected as giant candidates from the Washington+DDO51 color-color diagram are denoted with stars (★). Giant candidates also observed spectroscopically are denoted with large open circles (○) if they are not RV members and filled circles (●) if they are members. Other “fill” stars observed are denoted with open triangles (△) if they are not RV members and filled triangles (▲) if RV members.

#### 4. RESULTS

The photometrically identified, most likely RGB and RC stars unambiguously reveal the bulk RV of each cluster, as shown by the RV distributions in the left panels (a–e) of Figure 4. Since these RGB and RC stars are the most likely to provide the “purest” samples of cluster members, we use these samples to define one measure of the mean cluster RV and

TABLE 6  
STELLAR RADIAL VELOCITIES — BH176 FIELD

Star	$\alpha_{2000.0}$	$\delta_{2000.0}$	$V$	$(V-I)$	TDR	$V_r$ (km s <sup>-1</sup> )	Error $V_r$ (km s <sup>-1</sup> )	Type <sup>a</sup>	Cluster Member?
140	15:38:46.54	-50:02:00.9	18.95	1.840	10.5	8.4	2.2	fill	Y
225	15:38:46.92	-50:03:11.0	19.81	1.734	6.5	-36.5	3.4	fill	N
1793	15:38:52.34	-50:06:15.6	18.08	2.126	11.1	-1.5	2.1	fill	N
3313	15:38:57.42	-50:03:01.9	18.99	1.847	6.5	28.4	3.4	RC	N
3332	15:38:57.51	-50:02:24.5	18.90	0.977	17.1	-40.0	1.4	HB	N
3994	15:38:59.47	-50:03:50.8	18.80	1.862	6.5	12.6	3.4	RC	Y
4190	15:39:00.03	-50:04:16.3	17.83	2.234	24.4	6.4	1.0	RGB	Y
4245	15:39:00.24	-50:01:33.1	19.16	0.904	24.4	15.7	1.0	HB	Y
4360	15:39:00.57	-50:02:17.0	18.94	1.850	8.4	9.9	2.7	RC	Y
5278	15:39:02.96	-50:00:14.5	18.91	1.831	5.7	30.4	3.8	ERGB	N
5988	15:39:04.69	-50:03:17.1	19.49	0.998	5.7	2.2	3.8	HB	Y
6194	15:39:05.14	-50:05:05.6	19.25	0.943	14.9	-77.5	1.6	HB	N
8251	15:39:10.10	-50:02:24.0	18.84	1.793	9.2	-0.5	2.5	RC	N
8468	15:39:10.47	-50:06:33.5	18.96	1.874	6.1	-6.8	3.6	ERGB	N
9312	15:39:12.70	-50:01:59.9	18.05	2.243	20.2	11.4	1.2	RGB	Y
9327	15:39:12.72	-50:03:49.6	18.99	1.841	6.9	16.9	3.2	RC	Y
10823	15:39:16.77	-50:02:20.4	18.93	1.901	7.8	19.0	2.9	ERGB	Y
14629	15:39:29.82	-50:00:41.2	18.33	1.906	20.2	-80.8	1.2	fill	N
15302	15:39:32.18	-49:59:51.1	17.53	2.319	10.5	34.4	2.2	fill	N

<sup>a</sup>Spectroscopic candidates as selected from the CMD.

“RGB” are stars along the RGB within the cluster radius.

“ERGB” are the same only selected from outside the cluster radius.

“HB” stars are Horizontal branch candidates.

“RC” stars are red clump candidates.

“Fill” stars are randomly selected stars from out side the cluster radius.

TABLE 7  
STELLAR RADIAL VELOCITIES — BERKELEY 20 FIELD

Star	$\alpha_{2000.0}$	$\delta_{2000.0}$	$M$	$(M-I)$	$(M-DDO51)$	TDR	$V_r$ (km s <sup>-1</sup> )	Error $V_r$ (km s <sup>-1</sup> )	Type	Member?
10308	5:32:13.32	0:10:19.1	17.53	1.213	+0.063	6.9	1.5	3.2	fill	N
10617	5:32:33.19	0:09:35.0	17.32	1.466	-0.061	9.2	0.1	2.5	ERGB	N
10645	5:32:34.72	0:15:38.9	17.33	1.385	-0.048	10.0	24.4	2.3	fill	N
10741	5:32:36.99	0:12:00.8	17.69	1.456	-0.015	6.5	74.5	3.4	RGB	Y
10745	5:32:37.66	0:17:04.8	17.95	1.259	-0.007	5.7	36.5	3.8	fill	N
10770	5:32:37.93	0:11:09.8	15.12	1.909	-0.064	35.3	75.5	0.7	RGB	Y <sup>a</sup>
10794	5:32:39.16	0:17:28.7	17.74	1.324	-0.009	7.8	77.9	2.9	fill	Y
10806	5:32:38.98	0:09:27.5	17.08	0.943	+0.032	8.1	35.3	2.8	HB	N
10810	5:32:39.20	0:10:31.3	16.00	1.503	+0.006	20.2	73.7	1.2	RGB	Y
10850	5:32:41.03	0:06:19.4	18.49	0.947	+0.026	5.7	17.7	3.8	fill	N
10851	5:32:41.53	0:10:02.9	16.25	1.522	-0.002	15.9	79.3	1.5	RGB	Y
10864	5:32:42.31	0:12:29.7	17.01	1.050	+0.032	5.7	30.8	3.8	HB	N
10940	5:32:46.55	0:08:42.2	17.90	1.405	-0.006	6.3	40.2	3.5	ERGB	N
10979	5:32:49.99	0:11:54.4	16.80	1.154	+0.013	13.9	32.5	1.7	HB	N
10980	5:32:50.43	0:16:12.7	15.46	1.736	-0.027	30.8	53.8	0.8	fill	N
11054	5:32:54.76	0:17:30.6	15.48	1.723	-0.254	30.8	52.6	0.8	fill	N
11058	5:32:54.62	0:10:49.5	17.62	1.519	-0.053	10.0	56.6	2.3	ERGB	N
11094	5:32:57.52	0:15:22.7	17.09	1.428	-0.019	7.2	31.2	3.1	fill	N
11158	5:33:01.22	0:09:07.3	18.19	1.295	-0.023	6.1	-24.3	3.6	fill	N
11285	5:33:10.66	0:07:53.7	17.92	1.430	-0.057	7.5	56.5	3.0	fill	N

<sup>a</sup>Star in common with Yong et al. (2005).

observed dispersion (the top values of Table 11 with subscript “RGB”).

With this version of the mean RV established for each cluster, we can search for other potential cluster members identified on the basis of similar RV. The RV histograms for all stars in the cluster fields with spectra are shown in the right panels (f-i) of Figure 4. When the left and right panels of Figure 4 are compared we see the usefulness of photometric pre-screening to identify the *best* cluster RGB candidates for these sparse, highly field star contaminated clusters: e.g., in the cases of BH176, Be20, and Sa1 the true RV of the cluster

would remain somewhat uncertain were only the RV distributions in the right panels available. We can now rederive bulk cluster RVs using all stars with RVs indicating likely cluster membership. For this purpose, we limit the cluster member range to  $\pm 7$  km s<sup>-1</sup> about the mean defined by  $V_{r,RGB}$ , values guided by the typical individual stellar RV errors and the small expected velocity dispersions of these systems ( $\sim 1$ -3 km s<sup>-1</sup>). Because of this imposed selection bias, the dispersions given in Table 11 should be interpreted only as a guide to the observed tightness of the RVs used to define the mean RV, not as the true intrinsic dispersions of the clusters. The

TABLE 8  
STELLAR RADIAL VELOCITIES — BERKELEY 29 FIELD

Star	$\alpha_{2000.0}$	$\delta_{2000.0}$	$V$	$(V-I)$	TDR	$V_r$ (km s <sup>-1</sup> )	Error $V_r$ (km s <sup>-1</sup> )	Type	Member?
201	6:52:53.40	16:49:12.5	15.73	1.001	15.9	39.2	1.5	fill	N
208	6:53:03.07	16:49:17.7	17.30	1.140	9.2	19.1	2.5	fill	N
246	6:52:50.76	16:49:39.2	17.28	0.991	7.8	121.2	2.9	fill	N
249	6:53:14.68	16:49:40.7	17.47	1.075	8.1	-0.5	2.8	fill	N
462	6:53:14.92	16:52:01.3	17.23	0.952	11.1	61.6	2.1	fill	N
482	6:52:50.68	16:52:17.5	16.41	0.960	13.9	-27.7	1.7	fill	N
523	6:53:25.94	16:52:38.9	17.67	1.021	6.1	49.2	3.6	fill	N
549	6:53:33.24	16:52:57.4	16.94	0.946	10.0	28.5	2.3	fill	Y <sup>a</sup>
725	6:53:32.80	16:54:26.1	16.43	1.236	22.1	31.4	1.1	fill	Y
822	6:53:01.47	16:55:01.9	16.30	1.121	20.2	27.4	1.2	RGB	Y <sup>b</sup>
868	6:53:03.87	16:55:15.9	14.66	1.588	35.3	27.5	0.7	RGB	Y <sup>b,c</sup>
870	6:53:23.49	16:55:16.8	17.21	1.123	11.1	67.2	2.1	fill	N
934	6:53:02.20	16:55:35.3	15.98	1.077	20.2	-11.2	1.2	RGB	N
948	6:53:08.06	16:55:40.7	16.68	1.058	9.2	29.1	2.5	RGB	Y <sup>d,c</sup>
996	6:53:06.50	16:55:53.1	17.49	1.066	7.5	32.5	3.0	RGB	Y
1000	6:53:04.37	16:55:54.3	14.37	1.781	30.8	26.4	0.8	RGB	Y <sup>b,c</sup>
1078	6:52:59.74	16:56:17.5	18.00	1.014	7.5	20.8	3.0	RGB	Y
1165	6:53:01.67	16:56:45.3	15.97	1.078	17.1	53.9	1.4	RGB	N
1294	6:53:31.24	16:57:51.2	16.57	1.056	17.1	8.4	1.4	fill	N
1295	6:53:21.37	16:57:52.3	15.81	0.990	17.1	47.6	1.4	fill	N
1324	6:53:26.45	16:58:07.1	16.30	1.095	15.9	4.2	1.5	fill	N
1426	6:52:49.66	16:58:57.0	15.93	1.182	30.8	25.8	0.8	fill	Y
1433	6:53:25.24	16:59:00.6	17.93	0.860	6.7	-17.7	3.3	fill	N
1437	6:53:12.25	16:59:01.3	16.77	1.126	18.5	24.7	1.3	fill	Y
1461	6:53:05.25	16:59:13.2	15.31	1.093	35.3	33.2	0.7	fill	Y

<sup>a</sup>Star with RV consistent with membership, thought due to CMD location probably a field star

<sup>b</sup>Star in common with Bragaglia et al. (2005).

<sup>c</sup>Star in common with Yong et al. (2005).

<sup>d</sup>Star in common with CBVMR.

mean RVs for the clusters using these enlarged samples are also given in Table 11 (middle values with subscript “all”). Note that while these RV values average over a larger sample of stars and therefore might be expected to give a more accurate measure of the mean cluster RV, it is also the case that a higher fraction of interloping field stars with similar RVs may enter, and perturb, the average.

The RVs we have calculated for the five clusters using the “RGB” and the “all” samples agree to within 2 km s<sup>-1</sup>, which is less than half the observed dispersions. These RVs also agree in general with other recent determinations for these clusters (bottom values, denoted as “pub” in Table 11), but an offset of unknown origin is also found for Sa1 (see §4.4 below). The CMDs and color-color diagrams for these clusters with observed and member stars marked are shown in Figures 5–8.

#### 4.1. Isochrone Matching

We match isochrones to our clusters while constraining the metallicity to spectroscopically determined values. We explore a range in metallicities centered on the spectroscopically determined value for each cluster. Additionally, our radial velocity data help clarify the actual positions of the cluster RGBs to improve model isochrone fits for each cluster. Through these techniques, we re-derive age and distance estimates for the clusters Be29, BH 176, and Sa1.

The derived CMDs for these three GASS candidate clusters are compared to theoretical isochrones from Girardi et al. (2000). We use as free parameters the cluster’s age,  $E(V-I)$ ,  $(m-M)_v$ , and  $[\text{Fe}/\text{H}]$ . We must stress that given the confused appearance of the CMDs for these sparse clusters in heavily contaminated backgrounds, especially for Sa1, we must be

careful not to over-interpret the results of these matches. Nevertheless, useful information can still be extracted from these comparisons, and it is a useful exercise to compare these results with previously published values. In the analysis that follows, visual matching of isochrones covering a range in ages and metallicities is carried out after simultaneously varying  $E(V-I)$  and the distance modulus  $(m-M)_v$  to get the best fit for any given combination of age and metallicity. We have used the following equation from Carraro et al. (1999):

$$[\text{Fe}/\text{H}] = \log_{10}(Z) + 1.72125 \quad (3)$$

to convert between the observed metallicities and the total metallicity  $Z$  values used for the Girardi et al. (2000) isochrones. Additionally, we tested Salasnich et al. (2000)  $\alpha$ -enhanced isochrone for Be29, see §4.3 below.

#### 4.2. BH176

We measure the first reliable RV for BH176 ( $V_{r,\text{all}} = 11.2 \pm 5.3$  km s<sup>-1</sup>) based on 9 stars. This measurement is significantly different and better than our single star measurement given in F04, which was of poorer quality and lower resolution than our new data.

The photometric data used for BH176 were obtained from Phelps & Schick (2003), where these authors carried out isochrone matching using Bertelli et al. (1994) isochrones. We rederive the cluster parameters for the same photometric dataset, but now use the isochrones from Girardi et al. (2000). Figure 9 shows the matched isochrones when we adopt  $Z = 0.008$  ( $[\text{Fe}/\text{H}] = -0.38$ ),  $Z = 0.019$  ( $[\text{Fe}/\text{H}] = +0.0$ ) and  $Z = 0.03$  ( $[\text{Fe}/\text{H}] = +0.20$ ), with clusters members, determined from the spectroscopy, marked as solid triangles. The best results are achieved for the highest of these metallicities,

TABLE 9  
STELLAR RADIAL VELOCITIES — BERKELEY 39 FIELD

Star	$\alpha_{2000.0}$	$\delta_{2000.0}$	$M$	$(M-I)$	$(M-DDO51)$	TDR	$V_r$ (km s <sup>-1</sup> )	Error $V_r$ (km s <sup>-1</sup> )	Type	Member?
20289	7:46:12.10	-4:39:05.3	15.26	1.549	-0.024	27.2	54.7	0.9	fill	Y
20332	7:46:13.37	-4:41:52.3	17.35	0.988	+0.024	7.2	34.7	3.1	fill	N
20362	7:46:14.97	-4:37:32.2	17.32	1.071	+0.044	5.9	68.0	3.7	fill	N
20429	7:46:16.55	-4:44:59.1	17.29	1.098	+0.037	8.1	79.1	2.8	fill	N
20552	7:46:21.67	-4:35:06.1	17.13	1.001	+0.034	5.5	55.2	3.9	fill	Y
20685	7:46:25.30	-4:40:33.9	17.17	1.305	-0.032	11.1	58.8	2.1	fill	Y
20729	7:46:27.25	-4:32:06.5	17.28	1.056	+0.031	6.1	34.4	3.6	RGB	N
20797	7:46:28.59	-4:38:35.4	17.56	0.947	+0.047	5.5	37.1	3.9	fill	N
20814	7:46:28.29	-4:46:47.8	17.73	1.081	+0.042	5.5	43.8	3.9	RGB	N
20899	7:46:30.39	-4:48:49.6	16.49	1.408	+0.019	11.1	-0.9	2.1	fill	N
20904	7:46:32.17	-4:33:17.0	17.21	1.121	-0.005	6.1	-3.9	3.6	fill	N
21054	7:46:34.82	-4:41:14.3	16.81	1.407	-0.039	14.9	53.5	1.6	RGB	Y
21087	7:46:35.61	-4:42:09.7	17.31	1.081	+0.028	6.1	61.3	3.6	RGB	N
21091	7:46:35.88	-4:40:38.9	16.90	1.057	+0.016	11.7	53.4	2.0	RGB	Y
21152	7:46:37.18	-4:40:11.4	14.33	1.626	-0.022	35.3	54.8	0.7	RGB	Y
21206	7:46:38.58	-4:39:21.6	16.49	1.421	+0.007	18.5	54.0	1.3	RGB	Y
21247	7:46:38.99	-4:41:56.1	15.09	1.561	-0.037	30.8	51.5	0.8	RGB	Y
21305	7:46:40.53	-4:38:17.0	16.62	1.373	+0.029	13.9	97.7	1.7	RGB	N
21322	7:46:39.98	-4:45:51.3	17.29	1.235	+0.034	7.5	67.7	3.0	fill	N
21365	7:46:41.27	-4:40:56.9	14.65	1.620	-0.023	22.1	54.8	1.1	RGB	Y
21366	7:46:41.45	-4:39:08.3	14.66	1.688	-0.017	35.3	50.9	0.7	RGB	Y
21426	7:46:42.49	-4:41:28.1	16.95	1.054	+0.030	7.2	59.4	3.1	RGB	Y
21432	7:46:43.30	-4:34:28.7	15.89	1.531	-0.138	30.8	16.0	0.8	fill	N
21471	7:46:43.90	-4:38:13.9	16.98	0.938	+0.035	9.2	43.6	2.5	RGB	N
21523	7:46:44.57	-4:40:21.9	16.73	1.405	-0.014	22.1	45.8	1.1	RGB	N
21530	7:46:44.52	-4:41:33.3	17.00	1.208	+0.024	5.3	55.5	4.0	RGB	Y
21574	7:46:45.05	-4:42:55.0	17.05	1.436	-0.007	12.4	50.1	1.9	RGB	Y
21589	7:46:45.18	-4:44:30.2	17.62	1.091	+0.015	8.1	45.3	2.8	RGB	N
21606	7:46:46.04	-4:38:58.4	16.57	1.423	-0.029	27.2	54.4	0.9	RGB	Y
21689	7:46:47.35	-4:37:08.8	17.14	0.997	-0.016	5.2	42.6	4.1	RGB	N
21695	7:46:47.99	-4:32:35.3	17.72	1.041	+0.033	6.1	-15.4	3.6	fill	N
21769	7:46:48.56	-4:39:09.1	16.96	1.401	-0.019	10.5	50.5	2.2	RGB	Y
21792	7:46:48.43	-4:44:46.8	16.32	1.450	+0.002	15.9	37.6	1.5	RGB	N
21815	7:46:49.13	-4:41:55.5	15.65	1.540	-0.029	24.4	55.8	1.0	RGB	Y
21912	7:46:50.77	-4:41:28.7	14.43	1.584	-0.017	35.3	58.9	0.7	RGB	Y
21925	7:46:51.15	-4:40:29.1	15.03	1.721	-0.038	35.3	58.2	0.7	RGB	Y
21977	7:46:51.78	-4:43:18.1	16.55	1.522	-0.004	22.1	86.4	1.1	RGB	N
21982	7:46:51.74	-4:44:16.5	16.40	1.599	-0.180	27.2	3.7	0.9	RGB	N
21985	7:46:52.21	-4:40:03.9	17.18	1.254	+0.007	5.9	36.0	3.7	RGB	N
22013	7:46:52.51	-4:41:14.5	14.71	1.588	-0.023	35.3	53.9	0.7	RGB	Y
22135	7:46:54.00	-4:47:51.6	17.36	1.170	+0.063	7.8	27.4	2.9	fill	N
22138	7:46:53.93	-4:48:52.8	16.47	1.368	+0.004	9.6	-35.3	2.4	fill	N
22144	7:46:55.21	-4:36:51.1	16.18	1.389	-0.003	13.9	56.3	1.7	RGB	Y
22154	7:46:55.11	-4:39:27.2	15.44	1.563	-0.026	30.8	57.3	0.8	RGB	Y
22252	7:46:58.01	-4:31:40.8	17.14	1.045	+0.023	6.7	170.5	3.3	fill	N
22519	7:47:02.87	-4:40:58.8	17.09	1.132	+0.031	7.8	72.7	2.9	RGB	N
22584	7:47:04.94	-4:35:42.3	15.83	1.509	+0.002	27.2	53.8	0.9	fill	Y
22603	7:47:04.88	-4:40:35.2	17.40	1.061	+0.027	10.0	75.4	2.3	RGB	N
22704	7:47:06.82	-4:48:46.7	17.15	1.183	+0.064	8.1	56.5	2.8	fill	Y
22869	7:47:12.28	-4:43:17.8	17.27	1.195	+0.014	7.2	61.9	3.1	fill	N
22943	7:47:15.64	-4:37:28.7	17.48	1.190	+0.028	8.8	75.8	2.6	fill	N
22989	7:47:16.75	-4:39:15.0	14.51	1.558	-0.004	30.8	55.8	0.8	fill	Y
23040	7:47:17.81	-4:44:14.4	14.87	1.823	-0.072	35.3	62.5	0.7	fill	N
23082	7:47:19.41	-4:42:17.9	17.43	1.088	+0.003	5.3	67.1	4.0	fill	N

which is also the most metal rich value available from Girardi et al. (2000). A range of ages (5.6 and 7.1 Gyrs) seems to match fairly well the MSTO, the slope of the RGB, and the position of the RC, suggesting the age is not well constrained photometrically. Outside this age range a poor match is obtained when trying to match these three CMD features simultaneously. An  $E(V-I)$  from 0.64 to 0.68 is therefore derived, resulting in a heliocentric distance of 15.2-15.8 kpc (Table 12). We find similar cluster parameters (based on our new isochrone matches with updated stellar evolution models) to those obtained by Phelps & Schick (2003) using the same photometry.

We agree with the findings of Forbes et al. (2004) that, based on current, *photometrically*-determined [Fe/H], BH176 does not seem to follow the GASS AMR, in fact it is quite the opposite. We have also noted that the RV for BH176 is also not strongly correlated to the GASS RV trend, so, collectively, the present evidence makes BH 176 unlikely to be a member of the putative GASS cluster system. Analysis of the RV find that it consistent with an object (open cluster) rotating with the flat rotation curve of the Galactic disk. However, this result could also be consistent with a globular cluster passing through the disk. If BH176 is found spectroscopically to have [Fe/H]  $\sim$  0.0, and it is actually a globular cluster (as it has



TABLE 10  
STELLAR RADIAL VELOCITIES — SAURER 1 FIELD

Star	$\alpha_{2000.0}$	$\delta_{2000.0}$	$M$	$(M-I)$	$(M-DDO51)$	TDR	$V_r$ (km s <sup>-1</sup> )	Error $V_r$ (km s <sup>-1</sup> )	Type	Member?
122	7:20:50.84	1:43:08.1	16.89	1.456	-0.089	11.7	11.7	2.0	fill	N
145	7:21:13.56	1:43:20.6	16.64	1.500	-0.050	5.3	88.7	4.0	fill	N
289	7:21:11.57	1:44:49.9	16.33	1.484	-0.114	12.4	-6.0	1.9	fill	N
290	7:20:46.03	1:44:52.3	17.07	1.601	-0.195	12.4	-27.2	1.9	fill	N
311	7:21:00.52	1:45:07.0	17.09	1.579	-0.001	11.1	76.1	2.1	fill	N
389	7:21:20.15	1:45:57.2	17.52	1.679	...	8.4	3.2	2.7	fill	N
521	7:20:52.79	1:47:19.4	16.96	1.430	+0.005	11.7	90.3	2.0	RGB	Y
538	7:20:58.83	1:47:31.2	17.20	1.577	+0.003	15.9	97.4	1.5	RGB	Y
572	7:20:54.89	1:47:53.2	16.66	1.491	-0.000	10.5	98.2	2.2	RGB	Y <sup>a</sup>
693	7:20:57.23	1:48:45.4	17.14	1.558	+0.000	5.2	95.3	4.1	RGB	Y <sup>a</sup>
706	7:21:14.49	1:48:54.0	17.30	1.461	-0.047	7.5	2.4	3.0	fill	N

<sup>a</sup>Star in common with CBVMPPR.

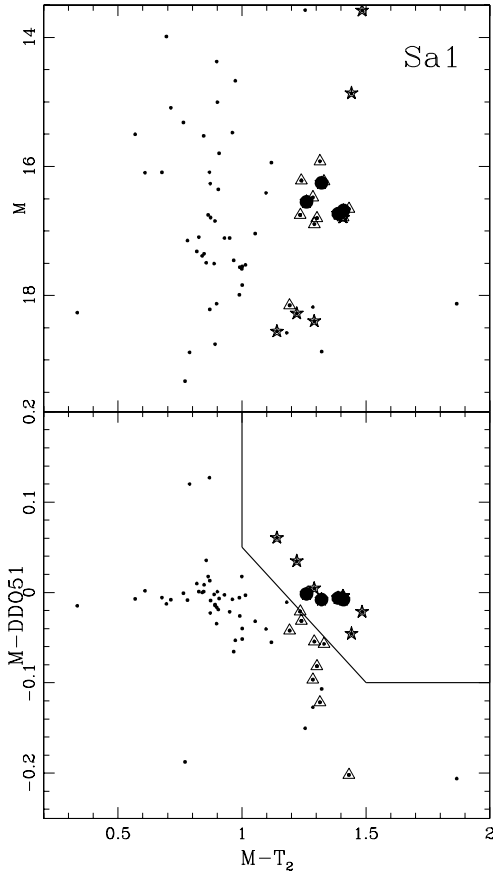


FIG. 6.— Same as Figure 9 for Sa1.

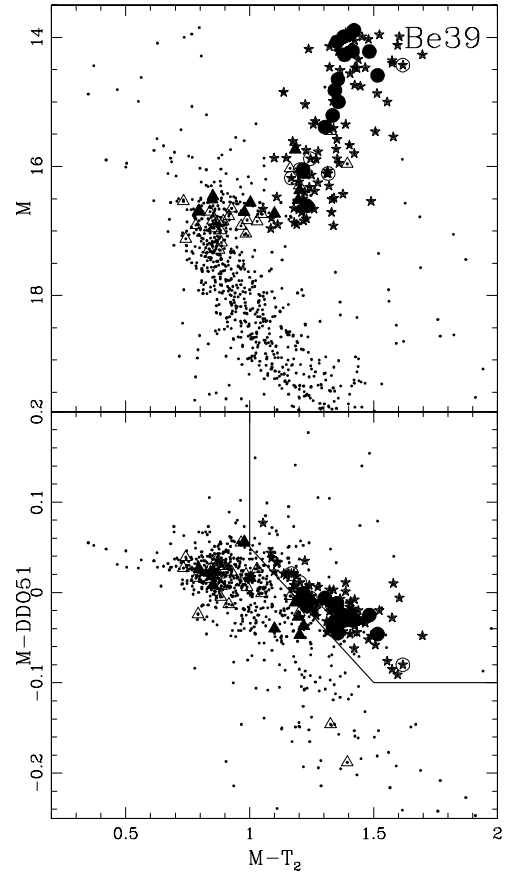


FIG. 7.— Same as Figure 9 for Be39.

been cataloged; Harris 1996), BH176 could provide important new constraints on Milky Way globular cluster formation scenarios.

#### 4.3. Be 29

The RV determinations for Be 29 is within the errors ( $1\sigma$ ) of other published findings (see table 11). For Be29, the measured spectroscopic metallicity is  $Z=0.005$  ( $[\text{Fe}/\text{H}] = -0.44$ ; Carraro et al. 2004, hereafter CBVMPPR). We explored  $Z=0.004$  ( $[\text{Fe}/\text{H}] = -0.68$ ),  $Z=0.008$  ( $[\text{Fe}/\text{H}] = -0.38$ ) and

$Z=0.019$  ( $[\text{Fe}/\text{H}] = +0.0$ ) Girardi et al. (2000) isochrones. Figure 10 shows the CMD for Be29 with the matched isochrones for the different adopted metallicities and for three different ages (3.2, 3.5 and 4.0) Gyrs. It is evident from the figure that both  $Z=0.004$  and  $Z=0.019$  isochrones do a poor job matching the slope of the RGB. The best matches are obtained for  $Z=0.008$ , and we can see that the three ages seem to do similarly well matching the rather poorly defined MSTO, subgiant branch, and position of the RC. Ages outside this range fail to reproduce the MSTO and the position of the

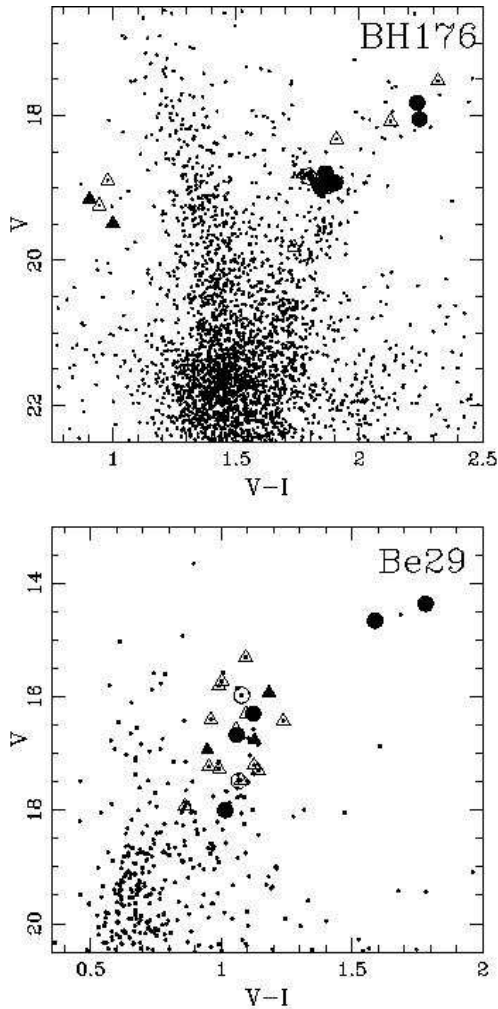


FIG. 8.— Be29 and BH176 VI photometry color-magnitude diagrams. Stars observed spectroscopically that were selected from the RGB in the core ( $\leq 2'$ ) are denoted with large open circles ( $\circ$ ) for non-members and filled circles ( $\bullet$ ) are for RV members. Triangles ( $\triangle$ ) are stars observed outside the cluster radius or non-RGB selected stars, again filled triangles ( $\blacktriangle$ ) denote stars selected as members.

RC simultaneously. Together, the isochrone matches suggest a probable age range of 3.2-4.0 Gyrs, and  $E(V-I)$  ranging from 0.08 to 0.10. These values yield a heliocentric distance of 13.1-14.5 kpc. The resulting “revised” cluster parameters (Table 12) are roughly consistent with previous work. We find a similar age, reddening and distance for Be29 to that found by Tosi et al. (2004), though we find a lower reddening and thereby farther distance when compared with Kaluzny (1994,  $E(V-I)=0.10$ ,  $d_{\odot} = 10.5$  kpc). Using the same isochrones for Be29 and Sa1, we find that Be29 is the most distant known open cluster ( $R_{GC} = 21$ ) in the Galaxy, as found by Tosi et al. (2004, see Table 12). The isochrone-fitted metallicity is in agreement, within our errors, to the spectroscopic, detailed chemical abundances of CBVMMPR and Yong et al. (2005).

However, Anthony-Twarog et al. (2005, hereafter AAT) pointed out in their comparison of NGC 2243 to Be29, that the findings of CBVMMPR show that Be29 is somewhat  $\alpha$ -enhanced. In Figure 11, we refit the CMD using the Padova  $\alpha$ -enhanced isochrones (Salasnich et al. 2000). AAT matched  $\alpha$ -enhanced isochrones to Be29 providing a reasonably good fit within previous determinations of the cluster reddening and

metallicity, although they do not have stars on the RGB higher than the RC. However as shown in Figure 11, our matches to  $\alpha$ -enhanced isochrones are markedly different. While some of the differences can be attributed to the different isochrones used, the primary difference comes from trying to match our 2 spectroscopically confirmed member stars above the RC. Matching the entire CMD with  $\alpha$ -enhanced isochrones requires one to make Be29 have solar  $[\text{Fe}/\text{H}]$ . While this match is consistent with previous reddening determinations, it is very inconsistent with previously determined *spectroscopic* metallicities which range from  $[\text{Fe}/\text{H}] = -0.4$  (CBVMMPR) to  $[\text{Fe}/\text{H}] = -0.7$  (Tosi et al. 2004). An additional method that comes near to matching the CMD, is to decrease the age to  $\leq 2.2$  Gyr, however this match is inconsistent with the finding of AAT, who find that the age difference of Be29 and NGC 2243 (Age =  $3.8 \pm 0.2$  Gyr) cannot be more than 0.5 Gyr. Additionally the reddening determined must be 50% higher than the highest previous estimate and double that found by AAT.

We find that Be29 cannot be consistently fit with  $\alpha$ -enhanced isochrones, therefore to account for the variable  $\alpha$  element enhancements found in CBVMMPR more complex models are needed. We refer the reader to §6.2 in Yong et al. (2005) for further discussion of the high resolution studies. Using the same isochrones for Be29 and Sa1 (see below), we find that Be29 is the most distant known open cluster ( $R_{GC} \geq 21$ ) in the Galaxy, as found by Tosi et al. (2004, see Table 12).

#### 4.4. Sa1

Our Sa1 RV ( $V_{r,all} = 95.4 \pm 3.6$  km s $^{-1}$ ) is smaller by  $\sim 9$  km s $^{-1}$  than the Sa1 velocity obtained by CBVMMPR. We note that two of our Sa1 stars — 572 and 693 — were the only stars observed by CBVMMPR for this cluster; CBVMMPR find RVs of (104.4, 104.8) km s $^{-1}$  for these two stars, respectively, while our survey finds (98.2, 95.3) km s $^{-1}$ . Thus, while both studies find small RV differences between the two stars, the relatively large RV offset between studies persists and is apparently not related to a difference in the stellar samples. While CBVMMPR does observe at much higher  $S/N$  than we do, the magnitude of the RV offset is significantly larger than the estimated uncertainty in the mean cluster motion for the two surveys. Moreover, we have found no net zero point offset in checks of our standard star RVs by comparison to the IAU values to our measurements, as shown in Table 4. The same template stars were used for the RV determination of all of the clusters and no large offset is found in Be20, 29, 39 or BH176. Thus, the origin of the systematic offset between the surveys is not clear. However, since we observed the same stars as CBVMMPR, we can determine that the four stars selected as members are indeed consistent with the work of CBVMMPR.

The sparse CMD of Sa1, and lack of bright giants, limits our ability to achieve a reliable isochrone match, though our RV members provide crucial benchmarks at the magnitude of the red clump. To improve the photometry depth and provide a better match, we used the photometry of Carraro & Baume (2003) within  $2'$  of the cluster center and added our confirmed members. The spectroscopic metallicity for Sa1 gives a  $Z = 0.008$  ( $[\text{Fe}/\text{H}] = -0.38$ ; CBVMMPR). We fit the ages 4, 4.5 and 5 Gyrs, with the fixed  $Z = 0.008$  metallicity, are studied as shown in Figure 13. An age of 4.5-5 Gyr is derived, since the 4 Gyr isochrones do not match well the MSTO. This match results in an  $E(V-I)$  that ranges from 0.19 to 0.24. The corresponding heliocentric distance for these val-

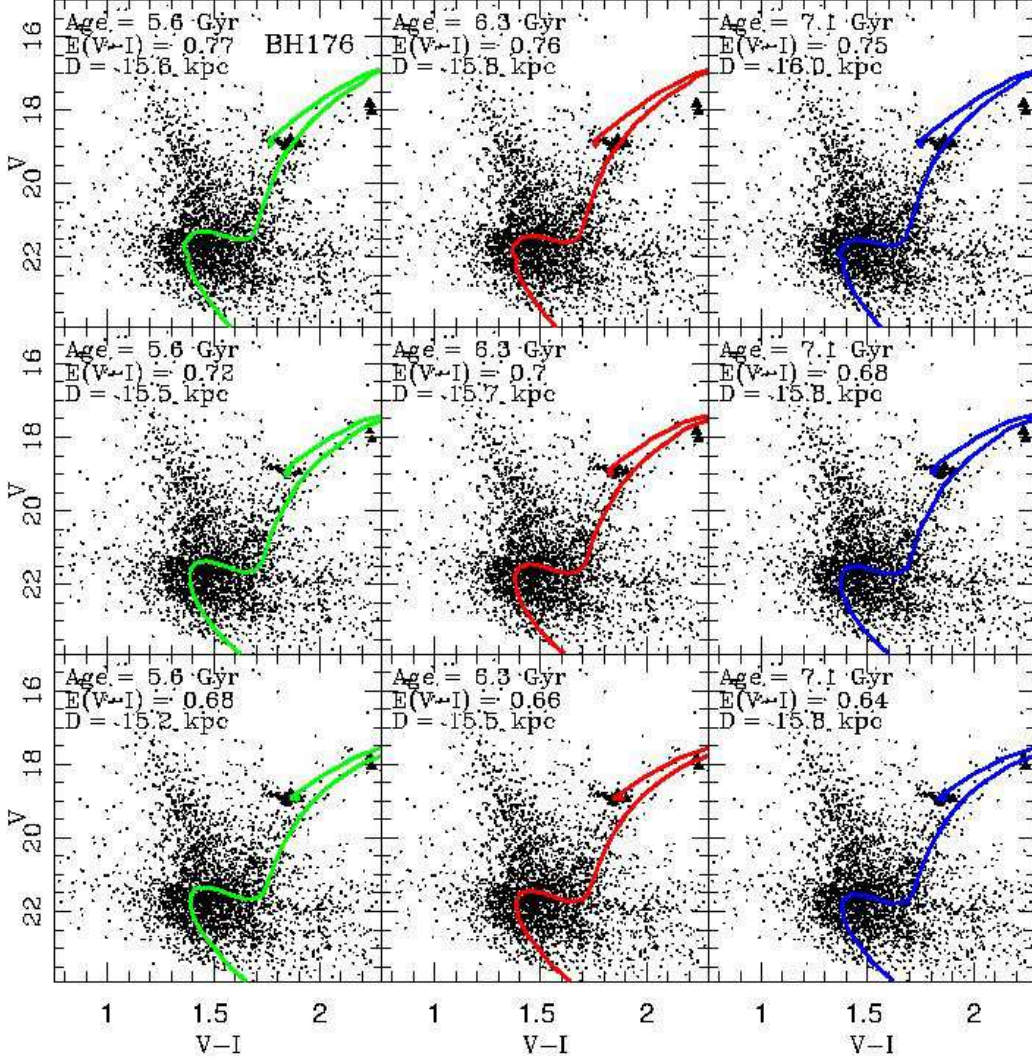


FIG. 9.— Girardi et al. (2000) isochrone matches for BH176. Metallicities of  $Z = 0.008$  ( $[\text{Fe}/\text{H}] = -0.38$ ),  $Z = 0.019$  ( $[\text{Fe}/\text{H}] = -0.0$ ), and  $Z = 0.030$  ( $[\text{Fe}/\text{H}] = +0.2$ ) are matched from top to bottom. Presumed cluster members, derived from spectroscopy are denoted with triangles ( $\blacktriangle$ ).

ues ranges from 11.8 to 13.5 kpc (see Table 12). We find that we are in relative agreement about the cluster parameters with other photometric studies of Sa1 (Frinchaboy & Phelps 2002; Carraro & Baume 2003). Frinchaboy & Phelps (2002) find an older age (6.3 Gyr) based on the morphological age index (Janes & Phelps 1994), which is known to yield older age estimates than those derived from isochrone matching.

#### 4.5. Cluster Membership

With defined “RV-member” samples, we may examine the membership reliability of stars selected to be cluster member candidates by our photometric pre-screening. This information is useful because a large number of our candidates have not been observed spectroscopically, but if we have confidence that the photometrically-selected candidates are likely to be members, they can potentially help constrain the likely positions of the RGB and RC sequences in the cluster CMDs as well as point to the effectiveness of these kinds of selections for picking spectroscopic samples in future studies. The RV membership success rate among Washington+DDO51 selected RGB stars with RVs is (100%, 53%, 100%) for (Sa1, Be39, and Be20) respectively. ERGB

stars were added to our analysis for Be20 but none were found to be members. The membership success rate for the *VI* selected RGB stars was 71% for BH176 (60% for RGB+RC+ERGB) and 75% for Be29. In previous studies of dwarf spheroidal galaxies (e.g., Westfall et al. 2005; Majewski et al. 2005), the Washington+DDO51 technique has been found to improve the selection reliability of star system RGB stars over CMD-only selection techniques by a significant factor, even with samples selected over larger areas, to the low density extremities of the clusters. The present use of the Washington+DDO51 technique is not completely analogous to these dSph studies, because here we have targeted *any* giant star candidates for spectroscopic follow-up without regard to CMD position (because in some cases the location of the RGB was not certain), whereas the dSph studies applied both Washington+DDO51 selected of giant candidates *and* specific CMD location pre-filtering on the stars samples. Nevertheless, we do find that use of the Washington+DDO51 filters has apparently improved our success rate relative to simply picking targets based on CMD position. For further discussion of the Washington+DDO51 selection technique the reader is directed to Majewski et al. (2000, 2005).

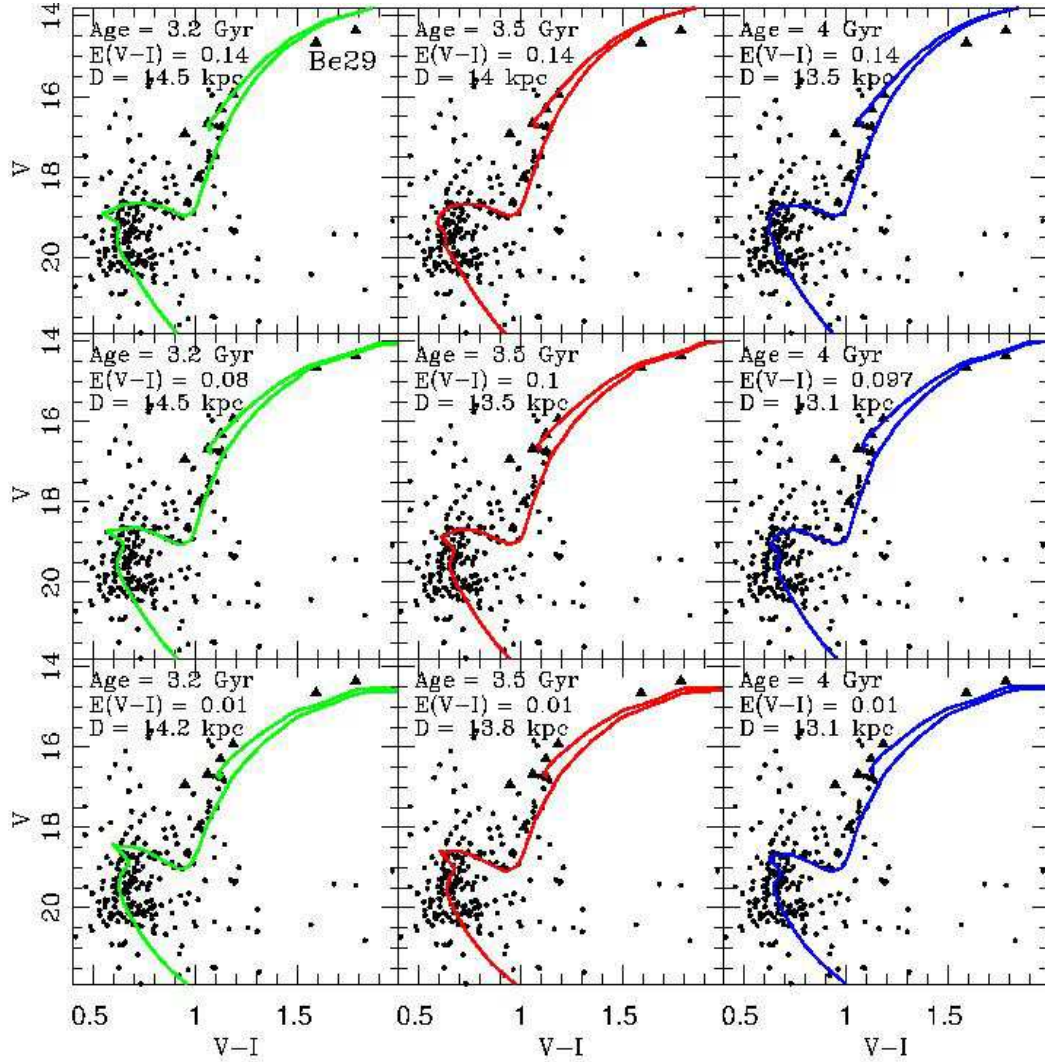


FIG. 10.— Girardi et al. (2000) isochrone matches for Be29. Metallicities of  $Z = 0.004$  ( $[\text{Fe}/\text{H}] = -0.68$ ),  $Z = 0.008$  ( $[\text{Fe}/\text{H}] = -0.38$ ), and  $Z = 0.019$  ( $[\text{Fe}/\text{H}] = -0.0$ ) are matched from top to bottom. Presumed cluster members, derived from spectroscopy are denoted with triangles (▲).

TABLE 11  
BULK CLUSTER RADIAL VELOCITIES

Cluster		BH176	Berkeley 20	Berkeley 29	Berkeley 39	Saurer 1
# Members	(RGB)	4	4	6	18	4
$V_{r,\text{RGB}}$	(km s <sup>-1</sup> )	9.1	75.6	27.1	55.0	95.4
$\sigma_{V_r,\text{RGB}}$	(km s <sup>-1</sup> )	4.6	2.5	3.8	2.9	3.6
$V_{\text{gsr},\text{RGB}}$	(km s <sup>-1</sup> )	-103.3	-22.0	-51.2	-107.1	-41.4
# Members	(all)	9	5	11	24	4
$V_{r,\text{all}}$	(km s <sup>-1</sup> )	11.2	75.7	28.4	55.0	95.4
$\sigma_{V_r,\text{all}}$	(km s <sup>-1</sup> )	5.3	2.4	3.6	2.5	3.6
$V_{\text{gsr},\text{all}}$	(km s <sup>-1</sup> )	-101.2	-21.8	-49.7	-107.1	-41.4
$V_{r,\text{pub}}$	(km s <sup>-1</sup> )	85.0 <sup>a</sup>	78.0	24.7	58.0	104.0
$\sigma_{V_r,\text{pub}}$	(km s <sup>-1</sup> )	30	5	0.1	2	0.1
Ref.		1	2	3	2	4

REFERENCES. — (1) F04; (2) Friel et al. (2002); (3) Yong et al. (2005); (4) CBVMPPR.

<sup>a</sup>RV based on one star, see §3.3

## 5. DISCUSSION AND CONCLUSIONS

The clusters Be29 and Sa1 have potentially critical leverage on radial, age and metallicity gradients in the Galactic

disk as determined by old open clusters (e.g., Carraro et al. 1994; Janes & Phelps 1994). Even with large statistical studies, most Galactic radial trends are highly dependent on the few open clusters in the extreme outer parts of the Milky Way



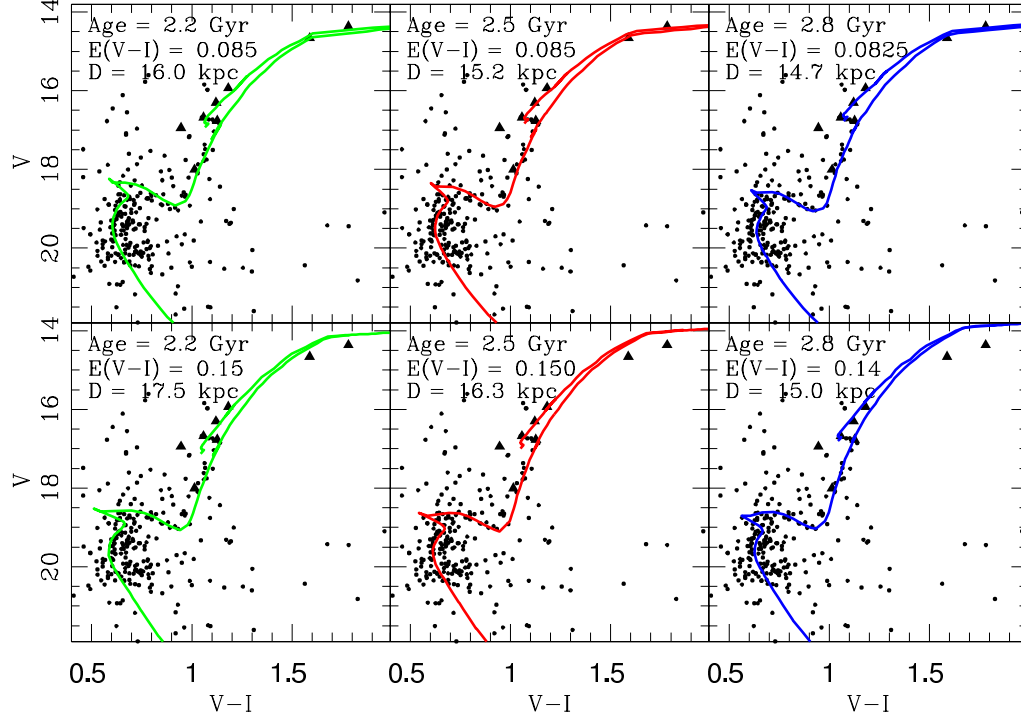


FIG. 11.— Salasnich et al. (2000) Padova  $\alpha$ -enhanced isochrone matches for Be29. Metallicities of  $Z = 0.008$  ( $[\text{Fe}/\text{H}] = -0.38$ ; bottom), and  $Z = 0.019$  ( $[\text{Fe}/\text{H}] = -0.0$ ; top) are matched. Presumed cluster members, derived from spectroscopy are denoted with triangles ( $\blacktriangle$ ).

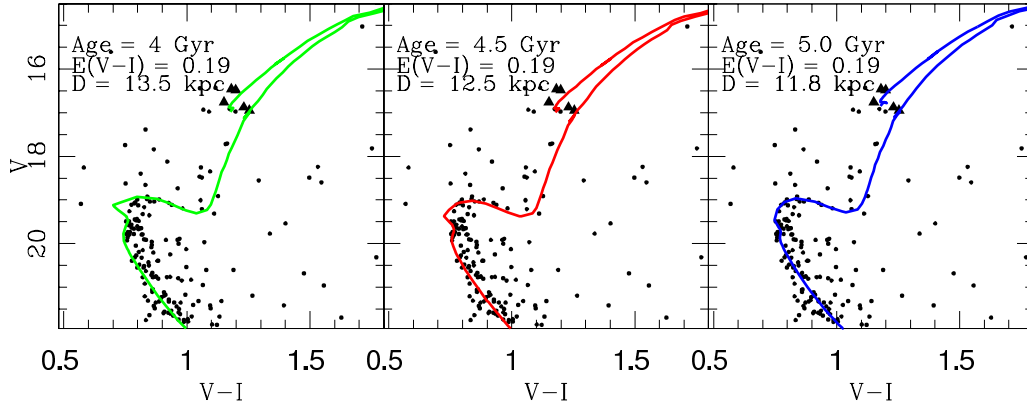


FIG. 12.— Girardi et al. (2000)  $Z = 0.008$  ( $[\text{Fe}/\text{H}] = -0.38$ ) isochrone matches for Sa1, using the Carraro & Baume (2003) photometry. Presumed cluster members, derived from spectroscopy are denoted with triangles ( $\blacktriangle$ ).

(Carraro et al. 1994; Friel et al. 2002). As discussed in CB-VMPR and Yong et al. (2005), these two outer clusters deviate from the radial-metallicity trend found for the rest of the bulk open cluster population by Friel et al. (2002), which suggests either that the chemical properties of the outer disk maybe different from the rest of the disk, or that these clusters have nothing to do with the chemical evolution of the disk. We explore the latter scenario now.

Friel (1995) has argued that the among the two most plausible models for the formation of the system of outer old open clusters, their creation as part of the normal secular evolution of the disk would require an unlikely “fine tuning” of formation and destruction processes. On the other hand, formation of these clusters through accretion is a “natural mechanism”

for forming these open clusters, which typically have large  $|Z_{GC}|$ . We find that, when viewed together, various properties of these old, outer open clusters lend circumstantial support to their being part of a tidal debris system, and may well be “accretion products” from GASS. We compare the derived cluster galactocentric radial velocities ( $V_{gsr}$ ) to the  $l$  vs.  $V_{gsr}$  trend found for the GASS M giants and other clusters (Crane et al. 2003, F04) in Figure 14. Included are the analytical fits to the stream from Figure 2 of the analysis by Penarrubia et al. (2005) for comparison. The following equation is used to convert from the  $V_r$  to  $V_{gsr}$  trend, as used in F04 and Crane et al. (2003):

$$V_{gsr} = V_r + 9 \cos(b) \cos(l) + 232 \cos(b) \sin(l) + 7 \sin(b) \quad (4)$$

TABLE 12  
BULK CLUSTER PARAMETERS

Cluster	Age(Gyr)	$d_{\odot}(kpc)$	$R_{gc}(kpc)$	$E(V-I)$	$[Fe/H]_{spec}$	$V_r(km\ s^{-1})$	$V_{gsr}(km\ s^{-1})$	GASS?
BH176	$6.3 \pm 1.0$	$15.8 \pm 0.5$	9.9	0.70	...	+11.2	-101.2	???
Berkeley 29	$3.7 \pm 0.5$	$13.4 \pm 0.4$	21.1	0.09	-0.44	+28.4	-49.7	Yes
Saurer 1	$4.5 \pm 1.0$	$13.1 \pm 0.4$	20.2	0.22	-0.38	+95.4	-41.4	Yes

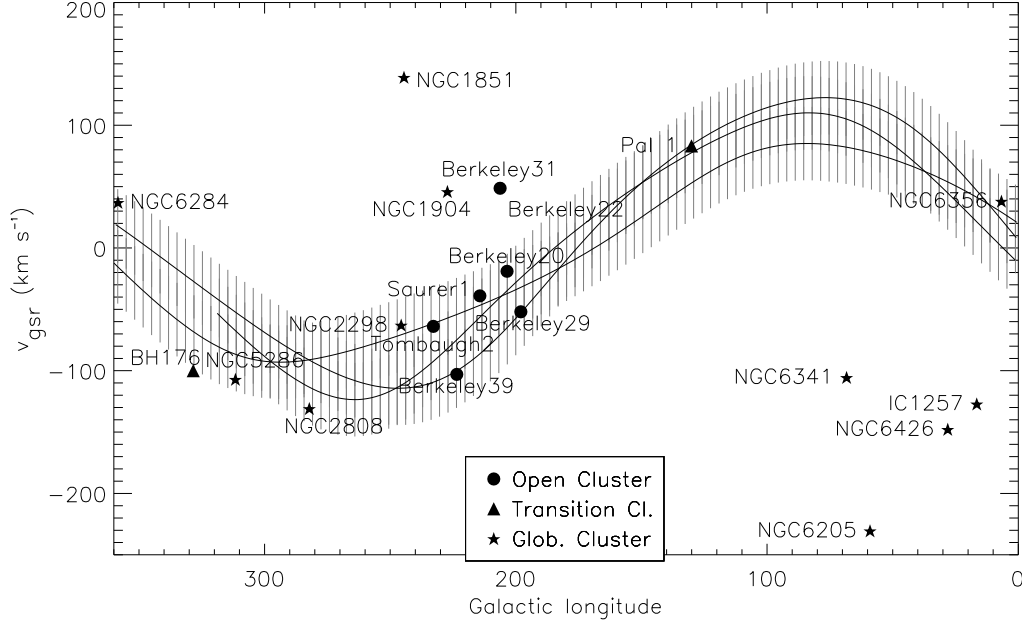


FIG. 13.— The  $l-V_{gsr}$  distribution of objects lying within 2.35 kpc of the GASS cluster plane and other clusters discussed in C03. Corrections to  $V_{gsr}$  are described in §3.2. The solid lines are analytical orbits for the Monoceros/GASS stream taken from Figure 2 of Penarrubia et al. (2005). The hash marks represent a velocity dispersion of  $30\ km\ s^{-1}$  about the  $V_{gsr}$  of the orbits, which approximately matches the velocity dispersion of GASS M giant stars from Crane et al. (2003).

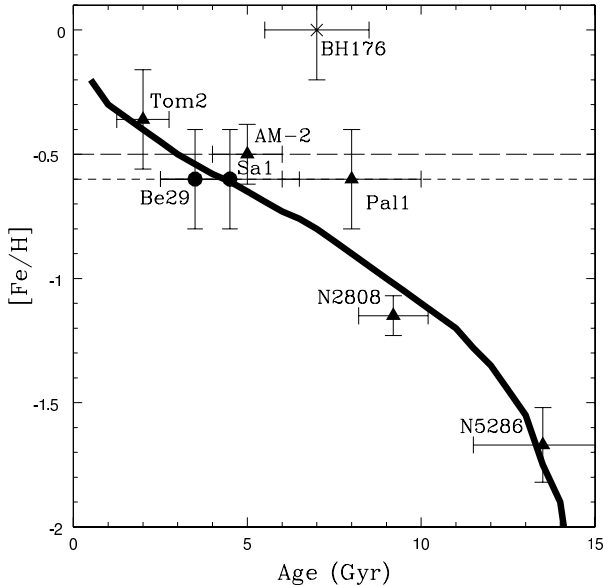


FIG. 14.— AMR for all GASS clusters with spectroscopically determined metallicities, and RVs consistent with membership, with circles (●) denoting Be29 and Sa1 with values from this study. The solid line is the AMR for the Sgr dSph (Layden & Sarajedini 2000). The dotted line shows the metal poor limit of the basically flat AMR for the Milky Way old open cluster system (Friel 1995). The (x) denotes BH176 based on its photometric metallicity that does not fit the GASS clusters AMR.

The RVs, when combined with the parameters in Table 11, yield a  $V_{gsr}$  of  $(-50, -39, -101)\ km\ s^{-1}$  for (Be29, Sa1, and BH176) respectively. These RVs place both Sa1 and Be29 within the GASS trend found in Crane et al. (2003) and, as shown in Figure 14, are generally consistent with the Monoceros models of Penarrubia et al. (2005). The new BH176 RV is only, at best, marginally consistent with membership in GASS. As pointed out by Penarrubia et al. (2005) and Yong et al. (2005), additional information, especially proper motions, are needed to test whether these clusters are part of a coherent dynamical group consistent with the GASS/Monoceros system.

Be 29 and Sa1 also follow the general age-metallicity trends suggested earlier for GASS (F04). We revisit (Figure 15) the GASS age-metallicity relation (AMR), now including only those clusters that are both spatially and dynamically consistent with GASS and for which *spectroscopic* metallicities have been derived: Be29, Sa1, Tombaugh 2, Arp-Madore 2, Palomar 1, NGC2808 and NGC 5286. In addition BH176 is included (shown as x) to show that if the isochrone metallicity is correct that it does not fit the AMR trend. Figure 14 also includes the AMR trend derived for the Sgr system (Layden & Sarajedini 2000) and the metal-poor “limit” to the old open clusters of the Galaxy (Friel 1995) shown as the long dashed lines. The Sgr trend is typical of that expected for an independently evolving, “closed-box” system

with protracted star formation, and it is clear that the proposed GASS cluster system more closely matches this Sgr AMR than the AMR of the nominal Milky Way open cluster system at smaller Galactocentric distances. We also compared to the metal poor envelope of the Carraro et al. (1998, small dashed line) AMR, which shows a “metal-poor spike” at  $\sim 3\text{--}4$  Gyr. However, all of the three clusters that are more metal-poor than  $[\text{Fe}/\text{H}] = -0.6$  have since had their metallicity re-evaluated and are found not to be as metal-poor. Still, it is interesting to consider that all of the clusters in this “spike” are all distant anticenter clusters, which requires one to ask whether this is due to a common formation, and if so what caused the “spike”

We conclude that the RVs of the clusters Sa1 and Be29 are consistent with GASS, which further points to an “accretion” origin for these clusters, if one believes that GASS represents an accreting dwarf galaxy system. But whether this “accretion” origin is by the cluster being taken in by the Milky Way already intact or by it being formed in the process of accretion cannot be distinguish with current data. The detailed abundances of Yong et al. (2005) and CBVMPP lend weight to outer disk clusters being formed *from* an accretion event, since the abundance ratios (specifically  $[\alpha/\text{Fe}]$ ) are too

high compared with current dwarf spheroidal galaxies. Be29 and Sa1 may be associated with the thick disk which also has enhanced  $[\alpha/\text{Fe}]$  (Venn et al. 2004) and could point to a common origin for both.

We thank the referee for their constructive comments that helped improve this paper. The authors would like to thank Eileen Friel for numerous useful discussions on this project. We would also like to thank Jeff Crane and Jorge Peñarrubia for help with comparisons to the GASS/Monoceros models. We also express gratitude to Marios Chatzikos, Sabrina Pakzad, Jennifer Pope, and Jason Buczyrna for their assistance with data collection in support of this project. This work was supported by NSF grant AST-0307851, NASA/JPL contract 1228235, and the David and Lucile Packard Foundation. PMF and RRM were supported by the F.H. Levinson Fund of the Peninsula Community Foundation. PMF was also supported by the Virginia Space Grant Consortium. RLP acknowledges support from a California State University, Sacramento Research and Creative Activity Award.

Facilities: Blanco(Hydra), Swope, FMO.

#### REFERENCES

- Amandroff, T. E. & Zinn, R. 1988, *AJ*, 96, 92
- Anthony-Twarog, B. J., Atwell, J., Twarog, B. A. 2005, *AJ*, 129, 872 (AAT)
- Bellazzini, M., Ferraro, F. R., & Ibata, R. 2003, *AJ*, 125, 188
- Bertelli, G., Bressan, A., Chiosi, C., Fagotto, F. & Nasi, E. 1994, *A&AS*, 106, 275
- Bragaglia, A., Held, E. V. & Tosi, M. 2005, *A&A*, 429, 881
- Carraro, G., Chiosi, C., Bressan, A. & Bertelli, G. 1994, *A&AS*, 103, 375
- Carraro, G., Ng, Y. K., Portinari, L. 1998, *MNRAS*, 296, 1045
- Carraro, G., Girardi, L., & Chiosi, C. 1999, *MNRAS*, 309, 430
- Carraro, G. & Baume, G. 2003, *MNRAS*, 346, 18
- Carraro, G., Bresolin, F., Villanova, S., Matteucci, F., Patat, F. & Romaniello, M. 2004, *AJ*, 128, 1676 (CBVMPP)
- Cenarro, A. J., Cardiel, N., Gorgas, J., Peletier, R. F., Vazdekis, A. & Prada, F. 2001, *MNRAS*, 326, 959
- Cenarro, A. J., Gorgas, J., Cardiel, N., Pedraz, S., Peletier, R. F. & Vazdekis, A. 2001, *MNRAS*, 326, 981
- Cole, A. A., Smecker-Hane, T. A., Tolstoy, E., Bosler, T. L. & Gallagher, J. S. 2004, *MNRAS*, 347, 367 (CSTBG)
- Crane, J. D., Majewski, S. R., Rocha-Pinto, H. J., Frinchaboy, P. M., Skrutskie, M. F., & Law, D. R. 2003, *ApJ*, 594, L119
- Dias W. S., Alessi B. S., Moitinho A., Lepine J. R. D., 2002, *A&A*, 389, 871
- Dean, J. F., Warren, P. R. & Cousins, A. W. J. 1978, *MNRAS*, 183, 569
- Forbes, D. A., Strader, J. & Brodie, J. P. 2004, *AJ*, 127, 3394
- Friel, E. D. 1995, *ARA&A*, 33, 381
- Friel, E. D., Janes, K. A., Tavares, M., Scott, J., Katsanis, R., Lotz, J., Hong, L. & Miller, N. 2002, *AJ*, 124, 2693
- Friel, E. D. 2005, in “Chemical Abundances and Mixing in Stars in the Milky Way and its Satellites”, eds. L. Pasquini & S. Randich, ESO Astrophysics Symposia
- Frinchaboy, P. M. & Phelps, R. L., 2002, *AJ*, 123, 2552
- Frinchaboy, P. M., Majewski, S. R., Reid, I. N., Crane, J. D., Rocha-Pinto, H. J., Phelps, R. L., Patterson, R. J., Muñoz, R. R. 2004, *ApJ*, 602, L21 (F04)
- Frinchaboy, P. M., Muñoz, R. R., Majewski, S. R., Friel, E. D., Phelps, R. L., & Kunkel, W. E. 2005, in “Chemical Abundances and Mixing in Stars in the Milky Way and its Satellites”, eds. L. Pasquini & S. Randich, ESO Astrophysics Symposia (astro-ph/0411127)
- Girardi, L., Bressan, A., Bertelli, G. & Chiosi, C. 2000, *A&AS*, 141, 371
- Geisler, D. 1996, *AJ*, 111, 480
- Harris, W. E., Fitzgerald, M. P. & Reed, B. C. 1981, *PASP*, 93, 507
- Harris, W. E. 1996, *AJ*, 112, 1487
- Helmi, A., Navarro, J. F., Meza, A., Steinmetz, M., & Eke, V. R. 2003, *ApJ*, 592, L25
- Ibata, R. A., Irwin, M. J., Lewis, G. F., Ferguson, A. M. N., & Tanvir, N. 2003, *MNRAS*, 340, L21
- Janes K. A. & Phelps, R. L. 1994, *AJ*, 108, 1773
- Kaluzny, J. 1994, *A&AS*, 108, 151
- Landolt, A. U. 1992, *AJ*, 104, 340
- Layden, A. C., & Sarajedini, A. 2000, *AJ*, 119, 1760
- Mackay, A. D. & Gilmore, G. F. 2003, *MNRAS*, 340, 175
- MacMinn, D., Phelps, R. L., Janes, K. A. & Friel, E. D. 1994, *AJ*, 107, 1806
- Majewski, S. R., Ostheimer, J. C., Kunkel, W. E., & Patterson, R. J. 2000, *AJ*, 120, 2550
- Majewski, S. R., Skrutskie, M. F., Weinberg, M. D., & Ostheimer, J. C. 2003, *ApJ*, 599, 1082
- Majewski, S. R., Frinchaboy, P. M., Kunkel, W. E., Link, R., Muñoz, R. R., Ostheimer, J. C., Palma, C., Patterson, R. J., & Geisler, D. 2005, *ApJ*, in press (astro-ph/0503627)
- Martin, N. F., Ibata, R. A., Bellazzini, M., Irwin, M. J., Lewis, G. F., Dehnen, W. 2004, *MNRAS*, 348, 12
- Momany, Y., Zaggia, S. R., Bonifacio, P., Piotto, G., De Angeli, F., Bedin, L. R., & Carraro, G. 2004, *A&A*, 421, L29
- Newberg, H. J., et al. 2002, *ApJ*, 569, 245
- Penarrubia, J., Martinez-Delgado, D., Rix, H.W. Gomez-Flechoso, M. A., Munn, J., Newberg, H., Bell, E. F., Yanny, B., Zucker, D., Grebel, E. K. 2005, *ApJ*, 626, 128
- Phelps, R. L. & Schick, M. 2003, *AJ*, 126, 265
- Rocha-Pinto, H. J., Majewski, S. R., Skrutskie, M. F., & Crane, J. D. 2003, *ApJ*, 594, L115
- Rocha-Pinto, H. J., Majewski, S. R., Skrutskie, M. F., & Patterson, R. J. 2005, *ApJ*, submitted (astro-ph/0504122)
- Salasnich, B., Girardi, L., Weiss, A., & Chiosi, C. 2000, *A&A*, 361, 1023
- Stetson, P. B. 1987, *PASP*, 99, 191
- Tonry, J. & Davis, M. 1979, *AJ*, 84, 1511
- Tosi, M., Di Fabrizio, L., Bragaglia, A., Carusillo, P. A. & Marconi, G. 2004, *MNRAS*, 354, 225
- Yanny, B., et al. 2003, *ApJ*, 588, 824
- Yong, D., Carney, B. & Teixeira de Almeida, M. L. 2005, *AJ*, in press (astro-ph/0504193)
- Venn K. A., Irwin, M., Shetrone, M. D., Tout, C. A., Hill, V. & Tolstoy, E. 2004, *AJ*, 128, 1177
- Vogt, S. S., Mateo, M., Olszewski, E. W. & Keane, M. J. 1995, *AJ*, 109, 151
- Westfall, K. B., Majewski, S. R., Ostheimer, J. C., Frinchaboy, P. M., Kunkel, W. E., Patterson, R. J., & Link, R. 2004, *AJ*, submitted